Nanoscale

Designing an ultrathin silica layer for highly durable carbon nanofibers as the carbon support in polymer electrolyte fuel cells

Journal:	*Nanoscale*
Manuscript ID:	NR-ART-07-2014-004293
Article Type:	Paper
Date Submitted by the Author:	29-Jul-2014

Complete List of Authors:	Hwang, Sun-Mi; Korea Institute of Energy Research, Fuel Cell Research Team Park, Jae-Hyun; Korea Institute of Energy Research, Fuel Cell Research Team Lim, Seongyop; Korea Institute of Energy Research, Fuel Cell Research Team Jung, Doo Hwan; Korea Institute of Energy Research, Fuel Cell Research Team Guim, Hwanuk; Korea Basic Science Institute, Division of Electron Microscopic Research Yoon, Young-Gi; Korea Institute of Energy Research, Hydrogen and Fuel Cell Center for Industry, Academy, and Laboratories Yim, Sung-Dae; Korea Institute of Energy Research, Fuel Cell Research Team Kim, Tae Young; Korea Institute of Energy Research, Hydrogen and Fuel Cell Center for Industry, Academy, and Laboratories

Designing an ultrathin silica layer for highly durable carbon nanofibers as the carbon support in polymer electrolyte fuel cells

Sun-Mi Hwang[a†], Jae-Hyun Park[a†], Seongyop Lim[a], Doo-Hwan Jung[a], Hwanuk Guim[b], Young-Gi Yoon[c], Sung-Dae Yim[a]*, Tae-Young Kim[c]*

A critical issue for maintaining long-term applications of polymer electrolyte fuel cells (PEFCs) is the development of an innovative technique for the functionalization of a carbon support that preserves their exceptional electrical conductivity and robustly enriches their durability. Here, we report for the first time how the formation of a partially-coated, ultrathin, hydrophobic silica layer around the surfaces of the carbon nanofiber (CNF) helps improve the durability of the CNF without decreasing the significant electrical conductivity of virgin CNF. The synthesis involved the adsorption of polycarbomethylsilane (PS) on the CNF's sidewalls, followed by high temperature pyrolysis of PS, resulting in a highly-durable, conductive carbon support in PEFCs. The Pt nanoparticles are in direct contact with surface of the carbon in the empty spaces between unevenly-coated silica layers, which are not deposited directly onto the silica layer. The presence of higher a Pt nanoparticle layer that was thicker over than the silica layer thickness would be a was quite advantageous circumstance for contacting in that it provided contact with other neighboring CNFs without having a significant adverse effect deeply damaging to on the electrical conductivity of the neighboring CNF composites with the silica layer. Furthermore, the ultrathin, hydrophobic silica layer around the surfaces of the CNF surfaces provides the provided great potential to reduce for reducing the presence s of water molecules in the vicinity of the carbon supports and the ·OH radicals formed on the surface of the Pt catalyst. As the a results, the CNF with 5 wt% silica layer that we prepared has had extremely high initial performance and durability in severe carbon corrosion conditions, starting up with 974 mA cm^{-2} at 0.6 V and ending up with more than 58 % of the initial performance (*i.e.*, 569 mA cm^{-2} at 0.6 V) after a 1.6 V holding test for 6 h. The beginning-of-life and end-of-life performances based on virgin CNF without the silica layer were 981 and 340 mA cm^{-2} at 0.6 V, respectively. The CNF that had a silica layer had long-term durability that was superior to that of the virgin CNF.

For the last decade, polymer electrolyte fuel cells (PEFCs), which have high energy conversion efficiency and are environmentally benign, have been recognized as a strong alternative power source with the potential for replacing the gasoline-powered internal combustion engine [1-4]. Among a number of composition factors, the development of cathode electrodes with acceptable durability is arguably the most important consideration for maintaining long-term automotive applications. This is due to the fact that their performances are typically limited by permanently damaged carbon supports and platinum (Pt) loss during abnormal and transient conditions, such as very fast potential transient conditions and frequent start-up/shutdown procedures [5-7].

More specifically, the amorphous carbon domains and the defective graphite crystallites in the carbon supports are preferentially corroded at low electrode potential (*i.e.*, $0.40 < E < 1.00$ V_{RHE}) during general PEFC operations. While, the graphitic domains of the carbon supports are susceptible to oxidation at high electrode potentials (> 1 V_{RHE}) during open-circuit voltage, start-up/shut-down processes, and fuel-starvation events [8]. For instance, the coexistence of H_2 and O_2 reactant gases within the anode side during frequent start-up/shut-down procedures at low temperature and localized water blockage (*i.e.*, anode flooding) can lead to conditions that corrode carbon at the cathode electrode. They also can cause severe performance losses through several mechanisms. In addition, two kinds of fuel starvation exist in PEFC operations. One is the local undersupply of the reactants while the gross supply at the cell level is sufficient, and the other is an overall undersupply of reactants at the total cell level. The former could induce corrosion of the cathode through the "reverse-current decay mechanism" [9], while the latter could result in catalyst degradation at the anode if the cell is connected in series with other cells and operates in the galvanostatic mode [10]. Hydrogen gas can be significantly depleted in the anode exhaust region during localized fuel starvation by the rapid cycling of the load. When this occurs the pressure at the anode side is relatively lower than that at the cathode side, so air will gradually diffuse into the anode side, creating an H_2/O_2 boundary. With overall fuel starvation, the cell potential declines significantly and even drives the cell into reverse operation, with the anode's potential being greater than the cathode's potential. This phenomenon entails water electrolysis and carbon oxidation at the anode in order to provide the protons and electrons required for the oxygen reduction reaction (ORR) that occurs at the cathode [11]. In addition, the Pt loss at the anode will directly reduce the H_2O_2 reduction reaction at the anode electrode and increase the H_2O_2 concentration in the polymer membrane, which results in severe degradation of the membrane during the operation of the fuel cell [12]. Furthermore, the excessive H_2 can consume the hydroxyl radicals at the catalyst of anode. Specifically, the adsorbed hydrogen atoms (H_{ad}) can react with hydroxyl radicals (·OH) and form water molecules ($Pt\text{-}H_{ad} + \cdot OH \rightarrow Pt + H_2O$), which reduces the degradation of the polymer

membrane by hydroxyl radicals [13]. Thus, it also is important to maintain the Pt content in the catalyst of anode.

In order to obtain the same power after severe carbon corrosion, the potential at the determined current would decrease gradually, leading to an increase in the amount of dissolved Pt [7]. This is because Pt dissolution is related closely to the formation and reduction of Pt oxides according to potential change. Since the potential is sufficiently negative to reduce Pt oxide, the Pt dissolution rate increases due to the reduction in the formation of the passive oxide layer. In addition, the considerable loss of Pt electro-catalysts at the cathode could accelerate the corrosion of the carbon cathode during start-up and shut-down procedures due to the decrease in proton transportation from the cathode to the anode side by the pseudo-capacitive effect according to: Pt-OH $\rightarrow$ Pt-O + H^+ + e^- [14, 15]. During the shut-down procedure, the Pt loss in the anode region could increase the corrosion of the carbon cathode by reducing the pseudo-capacitive effect that occurs at the anode side *via* the following reaction: Pt-H + H_2O $\rightarrow$ Pt-OH + H^+ + e^-. Thus, it also is important to maintain the Pt content in the anode catalyst layer. It follows from what has been said that carbon corrosion is correlated directly with Pt loss, as described in scheme 1. Hence, a highly-durable carbon support is essential for overcoming these limitations.

In the carbon corrosion procedures, the oxidation of carbon to form CO_2 is known to be dependent strongly on the water molecules and the Pt catalyst in the vicinity of the carbon support. Carbon surfaces with defect sites (*C**) are prone to form unstable C-OH groups *via* reversible electrochemical oxidation at a potential of 0.207 V_{RHE} [16]. The unstable surface C-OH groups can be oxidized further to form a stable C=O group at a potential of 0.8 V_{RHE}. At a higher potential of 0.95 V_{RHE}, the unstable C-OH groups are oxidized to form CO_2, creating a new defect site. In these procedures, the presence of water molecules plays a pivotal role in the mechanism of electrochemical carbon corrosion [17]. Since water is the primary oxidant during the accelerated stress test (AST), the implication is that having more water in the cathode catalyst layer would accelerate corrosion. Conversely, the absence of water molecules in the vicinity of carbon support would enhance the durability of the carbon support.

$$C^* + H_2O \leftrightarrow C\text{–}OH + H^+ + e^- \qquad E = 0.207\ V_{RHE} \quad (1)$$

$$C\text{–}OH \leftrightarrow C{=}O + H^+ + e^- \qquad E = 0.8\ V_{RHE} \quad (2)$$

$$C^*\text{–}C\text{–}OH + H_2O \rightarrow C^* + CO_2 + 3H^+ + 3e^- \qquad E = 0.95\ V_{RHE} \quad (3)$$

Carbon corrosion is catalyzed by contact with Pt in the electrodes. The transient species, such as the ·OH radicals formed on the surface of Pt catalyst, spill over to the carbon, resulting in formation of carbon oxide groups, which then proceed to CO_2. This means that the electrochemical corrosion of the carbon is accelerated by the presence of the Pt electro-catalyst [5, 16-19]. More specifically, the OH groups formed on the surface of the Pt can spill over to the surface of the carbon where they form ·OH radicals that are adsorbed on the surface of the carbon. The adsorbed ·OH radicals react with carbon defect sites (*C**) with unstable C-OH groups, resulting in the formation of CO_2 and creating a defect site as follows:

$$Pt + H_2O \leftrightarrow Pt\text{-}OH + H^+ + e^- \qquad E = 0.7\ V_{RHE} \quad (4)$$

$$Pt\text{-}OH + C \leftrightarrow Pt + C(\cdot OH)_{ads} \quad (5)$$

$$C\text{–}OH + C(\cdot OH)_{ads} \rightarrow C^* + CO_2 + 2H^+ + 2e^- \qquad E = 0.2\ V_{RHE} \quad (6)$$

Three reactions occur on the surface between the Pt and carbon. The first reaction to occur is the carbon oxidation reaction, described by reactions 1, 2, and 3. Second, the Pt is oxidized as described by reaction 4. Third, the Pt-OH reacts with the unstable surface oxide of carbon, C-OH, to form CO_2 and a carbon defect site, as shown in the following reaction:

$$C^*\text{–}C\text{–}OH + Pt\text{-}OH \rightarrow C^* + CO_2 + Pt + 2H^+ + 2e^- \qquad E = 0.65\ V_{RHE} \quad (7)$$

Therefore, it is important to have an appropriate strategy that provides a means of reducing carbon corrosion significantly, as follows: *i*) there must be fewer water molecules in the vicinity of the carbon supports to decrease the carbon corrosion and Pt oxidation according to the mechanism of electrochemical carbon corrosion; *ii*) the spill-over of ·OH radicals from the Pt particles must be minimized by avoiding direct contact between the oxidized Pt and the carbon surface.

Herein, we have reported a new strategy to functionalize the graphitized platelet carbon nanofiber (PCNF) surface, which was developed to make an unevenly-coated, ultrathin, hydrophobic silica layer on the PCNF. Subsequently, Pt nanoparticles would be deposited into an empty space between unevenly-coated silica layers, as shown in Fig. 1A and 1J. We can expect that *i*) the non-uniform coverage of the ultrathin silica layer would decrease the carbon corrosion by blocking the direct access of water molecules to defective carbon sites that are most susceptible to corrosion without decreasing the significant electrical conductivity of virgin PCNF. The increase in the hydrophobicity of PCNF with the surface of the silica layer would help to reduce the water content in the vicinity of the carbon support, resulting in enhanced durability of the carbon. Furthermore, the Nafion binder is the only contact with the hydrophobic silica layer and the Pt nanoparticles, so carbon corrosion at the interface between the Nafion binder and the surface of the carbon was diminished due to the decrease in the water transport *via* the Nafion binder in the vicinity of the carbon supports; *ii*) the electrical conductivity of the carbon support with an ultrathin silica layer was not affected significantly. This was primarily due to the presence of an efficient electron path from the carbon support to the Pt nanoparticles that were deposited into the empty gaps between the silica layers, as shown in Fig. 1A and 1J. Herein, we closely observed the overall surface of PCNF with an ultrathin silica layer. As a result, we confirmed that the Pt nanoparticles were in direct contact with the surface of the carbon, and the height of the Pt nanoparticle deposited directly onto the PCNF was slightly greater than that of approximately 2.4 ± 0.2 nm ultrathin silica layer. The fact that the Pt nanoparticle was thicker than the silica layer was a quite advantageous circumstance for contacting with other neighboring PCNFs without adversely affecting the electrical conductivity of the neighboring PCNF composites with the silica layer; and *iii*) the ultrathin silica layer on the PCNF helps counteract the effect of the spill-over of ·OH radicals from the surface of the oxidized Pt on carbon corrosion, which results in high cell performance even after severe carbon corrosion.

To date, it has been reported that the high ohmic resistance

associated with low electrical conductivity is the most controversial aspect of the carbon composites with a silica layer. For instance, the thick silica layer (*i.e.*, silica weight content > 40 wt%) that envelopes the Pt particles deposited on carbon nanotube (CNT) was developed to increase the stability of the Pt nanoparticles during voltage cycling [20, 21]. These previous studies reported that the thick silica layer was synthesized by hydrolysis and condensation of 3-aminopropyl-triethoxysilane (APTES) and/or tetraethoxysilane (TEOS). APTES can be uniformly adsorbed on the surface of the carbon support due to effective interaction between its amine groups and the functional groups of the carbon's surface. In addition, TEOS could be used to form a more complete silica layer on the pre-formed silica layer without any uncoated-silica sites. However, an important point to emphasize is that a silica content greater than 40 wt% was inadequate to meet the high electrical conductivity requirement of the carbon support due to the insulating property of the silica layer. In addition, the silica coating procedure after Pt deposition on CNT has several flaws, including ineffective oxygen and proton transport from the bulk phase to the Pt active sites [20-22]. Therefore, its beginning-of-life (BOL) and end-of-life (EOL) performances were significantly inferior to those of Pt/CNT without a silica layer, despite the fact that its durability was very superior.

In our work, polycarbomethylsilane ($[Si(CH_3)HCH_2]_n$) (PS) dissolved in the toluene solution was adsorbed uniformly onto the modified surfaces of the PCNF, and, then, the heat decomposition of PS was conducted to make an ultrathin, hydrophobic silica layer of 5 wt% on the surface of the PCNF using air gas at 400 ^oC and N_2 gas at 700 ^oC. Finally, Pt particles were deposited into the narrow space between the uncovered silica layers. Specifically, we conducted a thorough examination of the structural characteristics along the entire sidewall of the PCNF with a silica layer. Fig. 1 shows that *i*) the thickness of the ultrathin silica layer that was formed was approximately 2.4 nm with partially uncovered-silica regions on the entire PCNF surface; *ii*) the Pt nanoparticles were not deposited directly onto the silica layer (*i.e.*, the Pt nanoparticles were in direct contact with the carbon's surface); *iii*) the height of the Pt nanoparticles deposited on the surface of the PCNF was slightly greater than the thickness of the silica layer; and *iv*) the PCNF composite with a 5 wt% silica layer was much more resistant to corrosion over time at high-voltage operation than the virgin PCNF without a silica layer. These structural characteristics have pivotal roles in the enhanced BOL and EOL performances as compared to those of the virgin PCNF-based membrane electrode assembly (MEA).

Although the electrical conductivity of the PCNF composite with a 5 wt% silica layer was somewhat less than that of virgin PCNF without a silica layer, Fig. 2 shows that the silica layer on the PCNF had essentially no influence on the high-frequency resistance (HFR). The high electrical conductivity of the PCNF composite with a silica layer was attributed to the formation of an electron path from the carbon support to the Pt particles and to effective electron transport from the carbon support to neighboring supports, which causes a BOL performance similar to that of MEA based on the virgin PCNF without a silica layer. Furthermore, an ultrathin silica layer would also help to achieve the high electrical conductivity. More specifically, the electrical conductivities of virgin PCNF and PCNF composite with a 5 wt% silica layer were 3.79 and 3.15 S cm^{-1}, respectively. The HFR values for virgin PCNF and the PCNF composite with a 5 wt% silica layer were 69.7 and 70.9 mΩ cm^2, respectively. In general, two strategies were used for silica functionalization of the carbon supports. One involved covalent functionalization of silica onto the sidewalls of the carbon materials using either silyl ether or silane derivatives [23-25]. Although covalent functionalization is a well-controlled process, it can seriously diminish the desirable electronic properties of carbon materials. The other strategy was to coat the carbon supports with silica using a non-covalent methodology. A recent theoretical study showed that a non-bonded, protective silica layer only weakly perturbed the electronic structure of the carbon material [26]. Therefore, for optimal performance, the existence of a protective silica layer on the carbon material should enable the retention of its desirable electronic and mechanical properties. The silica coating did not interfere with the electrical properties of the carbon material. The methods used in the present work had several advantages over prior methods. For instance, the silica is coated on the carbon materials in a non-covalent fashion, making it a non-destructive process. In addition, the methods are fairly mild and environmentally-friendly in that they require a minimum amount of reactants, and the conditions that are used are neither harshly acidic nor basic.

More specifically, the formation of an ultrathin silica layer involved two major steps: *i*) hydrolysis of PS and further condensation of $Si(OH)_x$ to form silicone (*i.e.*, Si–O–Si) at 400 ^oC in air and *ii*) silicone transformation by pyrolysis at 700 ^oC in N_2 into amorphous Si–O–N onto the carbon matrix through the elimination of organic moieties and the release of other volatile compounds. The latter leads to an increase in hydrophobicity of the ultrathin silica layer mainly due to the transformation of the hydroxyl groups of Si–OH into Si–O–N during pyrolysis at 700 ^oC in N_2 gas [27, 28]. We confirmed the coordination environment of the ^{29}Si nuclei of the PCNF composite with a silica layer through solid-state ^{29}Si NMR. In addition, there were no Si resonances observed at ~ – 93.5 ppm (*i.e.*, HO–Si–$(O–Si)_3$) or – 103.2 ppm (*i.e.*, $(HO)_2$–Si–$(O–Si)_2$) in the ^{29}Si spectra, confirming that there were no Si-OH groups (data not shown). This indicates that the transformation of hydroxyl groups of Si-OH to form Si-O-N can be achieved *via* a pyrolysis procedure at high temperature in a N_2 gas environment. Specifically, the XPS results showed contributions from peaks at 400.6 and 402.5 eV, which were attributed to an additional oxygen atom bonded to nitrogen, such as O_2=N–Si and O–N=Si_2 (Fig. 3). The high-resolution Si 2p spectrum showed a peak located at 103.5 eV, which can be attributed to the SiO_2 signal, resulting from a siloxane network (Si–O–Si) of bonds originating from the condensation of silane molecules. Furthermore, the apparent absence of either Si–O–C or Si–C bonding suggested that the silica was attached to the surface of the carbon material *via* non-covalent functionalization. Thus, we believe that a thin silica layer would not interfere with the electrical conductivity of the original PCNF bulk. Surface hydroxyl groups help to retain water molecules *via* hydrogen bonding, so their disappearance is desirable to remove the water molecules from the surface of the PCNF. As shown in Fig. 4, we simply verified the increase in the

hydrophobicity of the PCNF composites with a silica layer by observing the variation in the weight of water adsorbed and/or absorbed in a PCNF composite determined by the results of water sorption isotherm measurements at given conditions of humidity and temperature. Fig. 4 shows that the water molecules adsorbed on the PCNF composite with a silica layer were low relative to the virgin PCNF material due to the disappearance of hydroxyl groups of Si–OH on the silica layer. However, this is a relatively small difference in mass of adsorbed water between them. This indicated that the more hydrophobic surface of the PCNF composite with a silica layer would not have a great effect on durability of the carbon support. However, the protective layer like an ultrathin silica layer would significantly reduce the direct contact of water molecules onto the overall surface of carbon, resulting to the increased durability of carbon support. Furthermore, the ultrathin silica layer on the PCNF helped counteract the adverse effect of the spill-over of ·OH radicals from the surface of the oxidized Pt on the corrosion of the carbon. This resulted in increased durability of the carbon support and the Pt particles during severe carbon corrosion. In this work, there were fewer water molecules in the vicinity of the carbon supports with the silica layer, which decreased the carbon corrosion according to the electrochemical carbon corrosion mechanism and decreased Pt oxidation. The interfacial double-layer capacitance region between 0.4 and 0.6 V in the cyclic voltammetry (CV) was used to easily understand the extent of damage to the carbon structure. Fig. 5B shows that the interfacial double-layer capacitance of the PCNF composite with a 5 wt% silica layer did not significantly change as did the virgin PCNF, which suggests that the PCNF composite with a 5 wt% silica layer was considerably more stable in this harsh condition. However, a significant increase in the amount of the interfacial double-layer capacitance of corroded virgin PCNF was believed to be due to an increase in the roughness of the carbon surface as well as the increased concentration of oxygen functionalities at the surface of the carbon support, because they are more hydrophilic and offer a greater capacitance [5, 29]. Furthermore, the current peaks, which corresponded to redox reactions of surface functional groups, were observed in the potential range between 0.5 and 0.7 V_{RHE} after carbon corrosion AST, with the most probable mechanism being a couple of redox reactions related to hydroquinone and quinone, as follows: C-OH (hydroquinone) ↔ C=O (quinone) + H^+ + e^- [5].

In the CV profiles during the AST procedure, the Pt reduction peak at around 0.8 V_{RHE} in the negative scan direction clearly shifted toward higher potentials, which reflected an increase of the average diameter of the Pt nanoparticles during the AST procedure [30]. The average diameter of the Pt nanoparticles obtained from the TEM images of the PCNF composite with a 5 wt% silica layer increased from 3.39 nm to 4.84 nm during the AST procedure (data not shown). The average diameter of the Pt nanoparticles deposited on the virgin PCNF without a silica layer significantly increased from 3.54 nm to 6.48 nm due to the migration and coalescence of Pt particles during severe carbon corrosion. The final, normalized electrochemical surface areas (ECSAs) of MEA based on PCNF composites with a 5 wt% silica layers were more than double those of MEA based on virgin PCNF without a silica layer. The double-layer capacitance of the PCNF composite with a 5 wt% silica layer did not significantly change with increasing time for carbon corrosion, as did the original PCNF without a silica layer. In the vicinity of the Pt nanoparticles supported on the carbon material, water molecules can infiltrate between the Pt and the carbon support, lowering the bonding energy of the metal/carbon support and facilitating the migration of Pt [31]. Thus, Pt particle growth is accelerated in a liquid environment, which is likely because the activation energy of Pt particle growth is decreased. As mentioned earlier, the abundant water molecules in the vicinity of the carbon's surface would accelerate the corrosion of the carbon, leading to a significant Pt loss during severe carbon corrosion. Thus, the presence of a more hydrophobic silica layer would be beneficial for enhancing the durability of the Pt nanoparticles and the carbon material. As a result, these characteristics increased the durability of the carbon supports and the Pt nanoparticles, and they also preserved the electrochemical activity of the Pt during the carbon corrosion condition.

The polarization curves that were determined experimentally during the AST under the constant high potential of 1.6 V_{RHE} were analyzed in stages to determine how carbon oxidation affected the total overpotential as the AST proceeded. The material prepared from PCNF with a 5 wt% silica layer had extremely high initial performance and durability in severe carbon corrosion condition, starting with 974 mA cm^{-2} at 0.6 V and ending with more than 58% of initial performance (*i.e.*, 569 mA cm^{-2} at 0.6 V) after a 1.6 V holding test for 6 h. On the contrary, the BOL and EOL performances based on virgin CNF without silica layer were 981 and 340 mA cm^{-2} at 0.6 V, respectively. Two significant observations can be made from Fig. 5: *i*) before carbon corrosion AST, the BOL performance based on PCNF composite with a 5 wt% silica layer was similar to that of PCNF without a silica layer primarily due to similar HFR values; to the best of our knowledge, its initial performance is one of the best among the PCNF composites with a silica layer reported in the literature and *ii*) after carbon corrosion AST, the EOL performance based on the PCNF composite with a 5 wt% silica layer was much better than the others. This indicated that the PCNF composite with a silica layer had long-term durability that was superior to that of the virgin PCNF; this superiority was due to the enhanced durability of the carbon supports and the Pt nanoparticles. In order to deeply scrutinize these experimental results, the total resistances, including kinetic loss (η_{kin}), HFR (η_{HFR}), proton resistance in cathode catalyst layers (η_{H^+}), and mass-transfer resistance (η_{mt}) were specifically obtained and shown in Figs. 5D and 5E. First, we concretely confirmed the Tafel slopes by variation of Pt electrocatalytic properties in order to give full details of these experimental results during carbon corrosion AST. Fig. 5D shows that the η_{kin} of the MEAs based on the PCNF composite with a 5 wt% silica layer were not significantly changed as a function of AST hold time as were those for the virgin PCNF-based MEA. (Data were corrected by measured HFR, proton resistance in the cathode catalyst layer, and H_2-crossover.) Due to these properties, η_{kin} associated with Pt electrocatalytic activity accounted for the largest contribution to the total overpotential of the PCNF composite with a 5 wt% silica layer, despite fact that the fraction of η_{kin} in the total overpotential did not increase significantly during the carbon corrosion AST.

Moreover, η_{HFR} and η_{H^+} of MEA based on the PCNF composite with a 5 wt% silica layer did not increase significantly over time during carbon corrosion AST. Consequently, it can be concluded that the ultrathin silica layer did not have a negative influence on proton and electronic conductivities, which leads to enhanced ORR activity of the residual Pt particles deposited on the ultrathin silica layer. Furthermore, unlike that of the virgin PCNF-based MEA, the η_{mt} of MEA based on the PCNF composite with a 5 wt% silica layer was not increased significantly because the less-corroded carbon layers maintained effective oxygen transport pathways to the active catalyst sites, primarily due to less collapse of the pore space. Simultaneously, the more-corroded carbon surfaces of the virgin PCNF supports were made more hydrophilic by roughening and by the addition of oxide groups on the surface, leading to an increase in the propensity of water flooding at the cathode side. These results led us to the conclusion that the proposed method of forming a uniform, ultrathin silica layer on the carbon supporting materials is the key to achieving significant increases in carbon durability and Pt activity.

Experimental Section

The entire surface of the virgin PCNF was modified by forming non-covalent π-π interactions between the sidewall of the graphitized PCNF and the phenyl moiety of toluene. More specifically, PCNF coated with a 5 wt% silica layer (CNF-100, Carbon Nano-material Technology Co., Ltd.) was fabricated using rota evaporation. A silica source consisting of 0.25 g of polycarbomethylsilane (MW 800, Sigma-Aldrich) was dissolved completely in 100 ml of toluene (anhydrous 99.9%, Sigma-Aldrich). PCNF of 4.75 g was well dispersed in the polycarbomethylsilane-toluene solution, and, then, the mixture was gently rotated overnight at room temperature using rotary evaporation. After removal of toluene by rota evaporation at 70 ^{o}C and 1000 rpm, the powdery Si/PCNF was annealed at 400 ^{o}C for 2 h in air flow of 200 cc min^{-1}, followed by ramping the temperature up to 700 ^{o}C and holding for 1 h in nitrogen flow of 200 cc min^{-1}. Subsequently, 40 wt% Pt on PCNF composite with a 5 wt% silica layer was prepared by the modified polyol method. The PCNF composite with a 5 wt% silica layer was well-dispersed in the solution of $PtCl_4$ (10% Pt, RTX) with DI water and 2-propanol (99.7%, Junsei Chemical Co., Ltd.). The carbonylation with CO gas (99.9%) was conducted for 3 h at room temperature under vigorous stirring to improve the distribution of Pt nanoparticles on the surface of PCNF. The slurry was refluxed at 90 ^{o}C for 3 h, and then the slurry was cooled down to room temperature. The Pt/PCNF with a 5wt% silica layer was filtered, washed, and dried at 70 ^{o}C for 24 h. In this work, although we have tried several times to control the patterns of silica layer, the formed silica layers had the irregular patterns. This is because the virgin PCNFs are all different shapes and sizes.

The anode catalyst ink was prepared by mixing commercial Pt supported on graphitized carbon (60 wt%, Johnson Matthey, HiSPEC 18600), 2-propanol, DI water, and a Nafion® D521 solution. The cathode catalyst ink was formulated with 40 wt% Pt deposited on PCNF composite with a silica layer, 2-propanol, DI water, and a Nafion® D521 solution. All cathodes and anodes had 30 wt% Nafion ionomer. MEA with an active area of 25 cm^2 was fabricated by the spray method on a 50-μm-thick Nafion NRE 212 membrane (DuPont). Anode and cathode Pt loadings were approximately 0.10 and 0.50 mg_{Pt} cm^{-2}, respectively.

The anode and cathode gases were humidified by passing them through bubbler-type humidifiers. Before the unit cell operation began, we calibrated the humidifiers of both the cathode and the anode by using a humidity sensor (Viasensor HS-1000). All single cell experiments were conducted at 70 °C, and the temperature of the gas lines to the anode and the cathode were always set 10 °C above the temperature of the humidifier to avoid the condensation of the water vapor. The polarization experiments were conducted in a galvanostatic mode, and an electronic load was used to maintain a constant current. At each current, the cell was allowed to stabilize for 18 min before the voltage of the cell was measured. At currents less than 10 A, the anode was fed with humidified H_2 gas at a constant flow rate of 100 mL min^{-1}, and the cathode was fed with humidified air at a constant flow rate of 410 mL min^{-1}, all at ambient pressure. At currents greater than 10 A, the stoichiometric quantities of H_2 and air were 1.43 and 2.5, respectively. The cathode and the anode were purged with N_2 (1500 mL min^{-1}) and H_2 (350 mL min^{-1}), and, then, cyclic voltammetry (CV) was performed to measure the electrochemical surface area (ECSA) of Pt using an electrochemical impedance spectroscopy potentiostat. The potential range and the scan rate were 0.04 – 1.2 V (vs. RHE) and 20 mV s^{-1}, respectively. We measured the proton resistance within the electrode by using a one-dimensional transmission-line model under an H_2-fed anode (reference/counter electrode) and a N_2-purged cathode (working electrode). The cathode and the anode were purged with N_2 (900 mL min^{-1}) and H_2 (900 mL min^{-1}), respectively.

The technology known as ^{29}Si solid-state NMR is a well-established means of determining the coordination environments of ^{29}Si nuclei, which provides the condensation degree of the silica network. Solid-state NMR spectra were recorded on a 400 MHz Bruker Avance spectrometer operating at a frequency of 80 MHz for the ^{29}Si nuclei and using the magic-angle spinning technique. The sample spinning rate was 10 kHz. The morphologies of the prepared samples were examined using a transmission electron microscope (TEM) (Titan Double Cs corrected TEM, FEI Co.) and ultra high resolution (UHR) field emission scanning electron microscope (FE-SEM) (MERLIN, Carl Zeiss). The surface compositions were measured using an X-ray photoelectron spectrometer (XPS) (K-Alpha, Thermo VG Scientific), equipped with a monochromatic Al K-α X-ray source (1486.6 eV).

Acknowledgments

This work was supported by the New & Renewable Energy Core Technology Program of the KETEP funded by the MTIE (20113020030020 and 20113010030090), Republic of Korea. H. Guim acknowledges the Korea Basic Science Institute grant T34619.

Notes and references

[a] *Fuel Cell Research Center, Korea Institute of Energy Research (KIER), Daejeon, 305-343, Republic of Korea.*
[b] *Division of Electron Microscopic Research, Korea Basic Science Institute (KBSI), Daejeon, 305-333, Republic of Korea.*
[c] *Hydrogen and Fuel Cell Center for Industry, Academy, and Laboratories, Korea Institute of Energy Research (KIER), Jellabuk-do, 579-841, Republic of Korea.*

**Corresponding author. E-mail: kty@kier.re.kr (T.-Y. Kim); Tel: +82-63-581-1672; Fax: +82-63-581-1630. ** Co-corresponding author. E-mail: jimmyim@kier.re.kr (S.-D. Yim); Tel: +82-42-860-3306; Fax: +82-42-860-3104. Sun-Mi Hwang and Jae-Hyun Park contributed equally to this work.*

† Electronic Supplementary Information (ESI) available: All experimental procedures and characterization of synthetic materials. See DOI: 10.1039/b000000x/

1. J. Y. Cheon, T. Kim, Y. Choi, H. Y. Jeong, M. G. Kim, Y. J. Sa, J. Kim, Z. Lee, T. Yang, K. Kwon, O. Terasaki, G. Park, R. R. Adzic, S. H. Joo, *Sci. Rep*., 2013, **3**, 2715.
2. M. K. Debe, *Nature*, 2012, **486**, 43.
3. A. S. Arico, P. Bruce, B. Scrosati, J. Tarascon, W. V. Schalkwijk, *Nat. Mater*., 2005, **4**, 366.
4. T. Kim, J. Lee, T. Yang, Y. Yoon, S. Park, S. Yim, *RSC Adv*., 2012, **2**, 6957.
5. J. Park, S. Yim, T. Kim, S, Park, Y. Yoon, G. Park, T. Yang, E. Park, *Electrochim. Acta*, 2012, **83**, 294.
6. J. D. Fairweather, D. Spernjak, A. Z. Weber, D. Harvey, S. Wessel, D. S. Hussey, D. L. Jacobson, K. Artyushkova, R. Mukundan, R. L. Borup, *J. Electrochem. Soc.,* 2013, **160(9)**, F980.
7. A. A. Topalov, S. Cherevko, A. R. Zeradjanin, J. C. Meier, I. Katsounaros, K. J. J. Mayrhofer, *Chem. Sci*., 2014, **5**, 631.
8. L. Castanheira, L. Dubau, M. Mermoux, G. Berthomé, N. Caqué, E. Rossinot, M. Chatenet, F. Maillard, *ACS Catalysis*, 2014, **4**, 2258.
9. Z. Y. Liu, B. K. Brady, R. N. Carter, B. Litteer, M. Budinski, J. K Hyun, D. A. Muller, *J. Electrochem. Soc.,* 2008, **155(10)**, B979.
10. X. Yang, Q. Ye, P. Cheng, *Int. J. Hydrogen Energy*, 2012, **37**, 14439.
11. S. Zhang, X. Yuan, H. Wang, W. Mérida, H. Zhu, J. Shen, S. Wu, J. Zhang, *Int. J. Hydrogen Energy*, 2009, **34**, 388.
12. C. Chen, T. F. Fuller, *Electrochim. Acta*, 2009, **54**, 3984.
13. Y. Chen, D. Li, X. Wang, L. Wu, X. Wang, X. Fu, *New J. Chem*., 2005, **29**, 1514.
14. S. Kreitmeier, A. Wokaun, F. N. Büchi, *J. Electrochem. Soc.,* 2012, **159(11)**, F787.
15. W. Gu, R. N. Carter, P. T. Yu, H. A. Gasteiger, *ECS transactions*, 2007, **11(1)**, 963.
16. A. Pandy, Z. Yang, M. Gummalla, V. V. Atrazhev, N. Y. Kuzminyh, V. I. Sultanov, S. Burlatsky, *J. Electrochem. Soc.,* 2013, **160(9)**, F972.
17. J. H. Kim, E. A. Cho, J. H. Jang, H. J. Kim, T. H. Lim, I. H. Oh, J. J. Ko, S. C. Oh, *J. Electrochem. Soc.,* 2010, **157(1)**, B104.
18. B. Wickman, H. Grönbeck, P. Hanarp, B. Kasemo, *J. Electrochem. Soc.,* 2010, **157(4)**, B592.
19. N. Linse, L. Gubler, G. G. Scherer, A. Wokaun, *Electrochim. Acta*, 2011, **56**, 7541.
20. S. Takenaka, H. Matsumori, H. Matsune, E. Tanabe, M. Kishida, *J. Electrochem. Soc.,* 2008, **155(9)**, B929.
21. H. Matsumori, S. Takenaka, H. Matsune, M. Kishida, *Appl. Cat. A: General*, 2010, **373**, 176.
22. S. Takenaka, H. Miyamoto, Y. Utsunomiya, H. Matsune, M. Kishida, *J. Phys. Chem. C*., 2014, **118(2)**, 774.
23. M. Bottini, L. Tautz, H. Huynh, E. Monosov, N. Bottini, M. I. Dawson, S. Bellucci, T. Mustelin, *Chem. Comm*., 2005, **6**, 758.
24. L. Vast, G. Philippin, A. Destrée, N. Moreau, A. Fonseca, J. B. Nagy, J. Delhalle, Z. Mekhalif, *Nanotechnology*, 2004, **15**, 781.
25. M. Aizawa, M. S. P. Shaffer, *Chem. Phys. Lett*., 2003, **368**, 121.
26. J. C. Wojel and S. T. Bromley, *J Phys. Chem. B*, 2005, **109**, 1387.
27. M. Narisawa, *Materials*, 2010, **3(6)**, 3518.
28. C. H. Kim, B. Kim, *Electrochim. Acta*, 2014, **117**, 26.
29. A. P. Young, J. Stumper, E. Gyenge, *J. Electrochem. Soc.,* 2009, **156(8)**, B913.
30. A. Zana, J. Speder, M. Roefzaad, L. Altmann, M. Bäumer, M. Arenz, *J. Electrochem. Soc.,* 2013, **160(6)**, F608.
31. M. P. Rodgers, L. J. Bonville, H. R. Kunz, D. K. Slattery, J. M. Fenton, *Chem. Rev*., 2012, **112**, 6075.

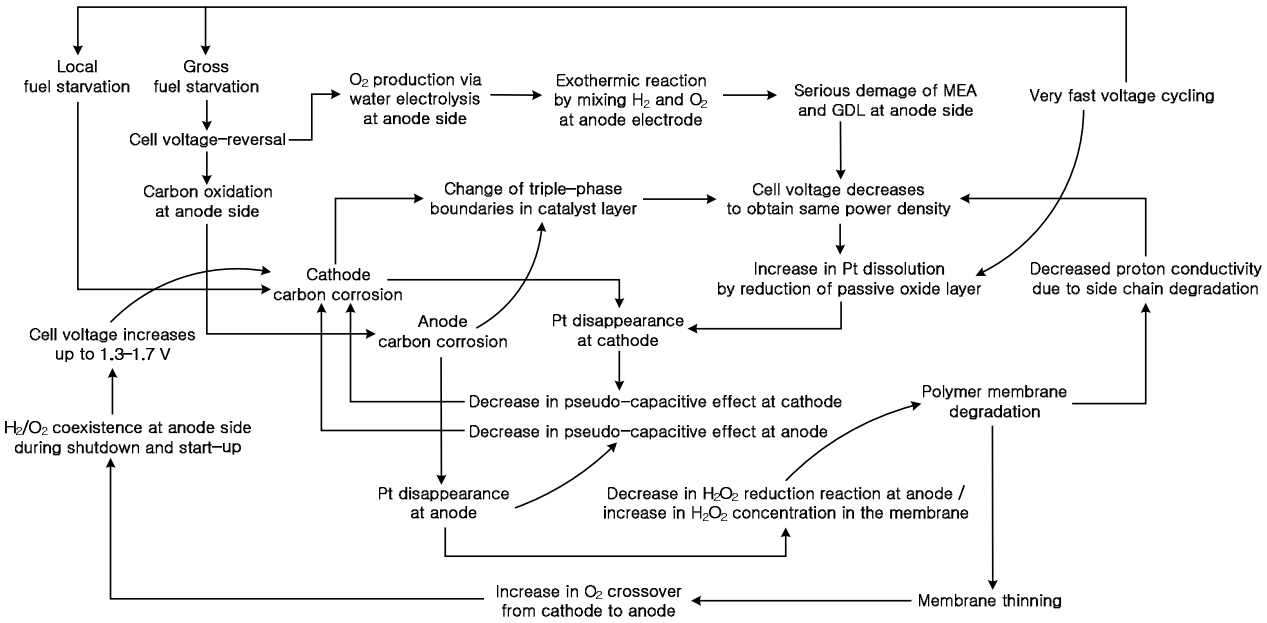

Scheme 1 Degradation characteristics of polymer electrolyte fuel cell caused by abnormal conditions and interconnections between different parts.

5

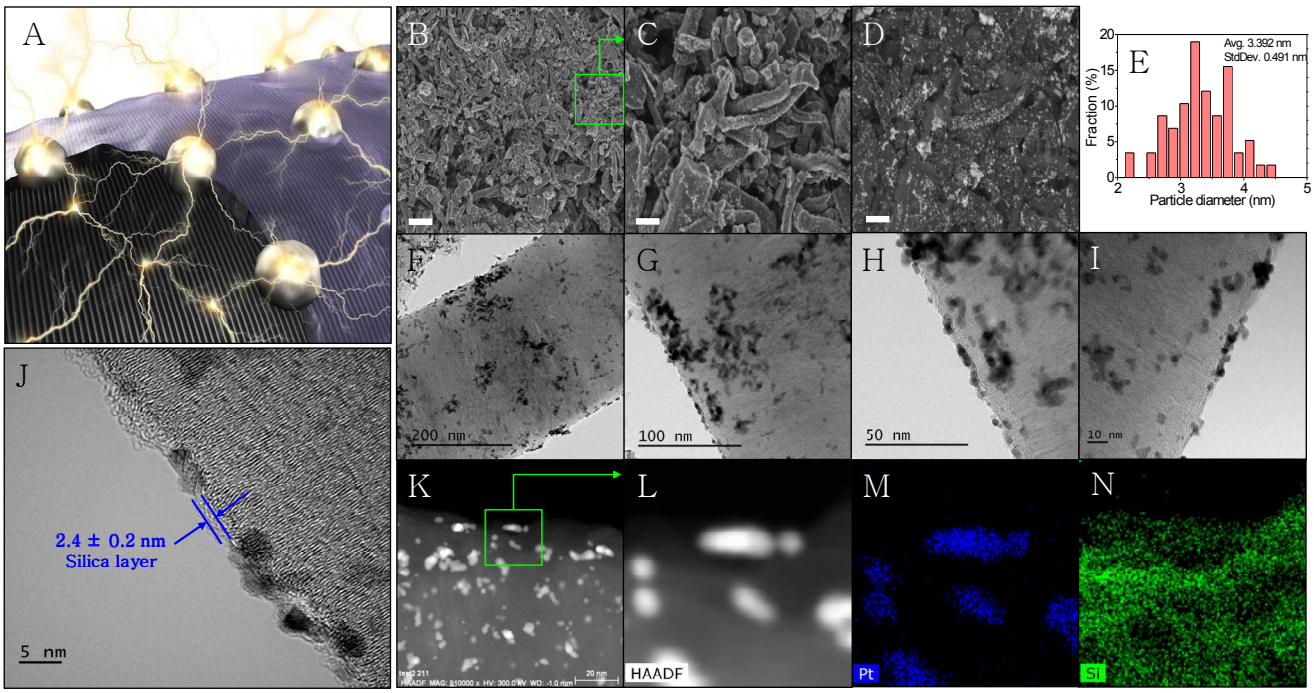

Fig. 1 Structure and characteristics of CNF with 5 wt% ultrathin silica layer. A, Schematic illustrating how a carbon nanofiber (CNF) with ultrathin silica layer enables to have a highly-conductive surface area. The silica layer (purple) is coated partially on the entire CNF surface (black). Pt nanoparticles (silver) are contacted directly with carbon surface in the empty spaces between unevenly-coated silica layers, which are not deposited directly onto the silica layer. Owing to these properties, the electrical conductivity of CNF with silica layer is similar with that of the original CNF without silica layer. **B to C,** Ultra high resolution FE-SEM images of carbon nanofibers in the cathode catalyst layer (Scale bar of B image, 1 μm; scale bar of C image, 200 nm). **D**, Backscattered electron (BSE) image of B (Scale bar, 200 nm). **E**, Pt particles diameter distribution on CNF with silica layer (Average of Pt particle diameter, 3.392 nm; Standard deviation, 0.491 nm). **F to J**, TEM images of CNF with silica layer. **K to L**, Dark-field TEM images of CNF with silica layer. **M to N**, Corresponding EDS elemental mapping of Pt (blue) and Si (green) in the region of L image.

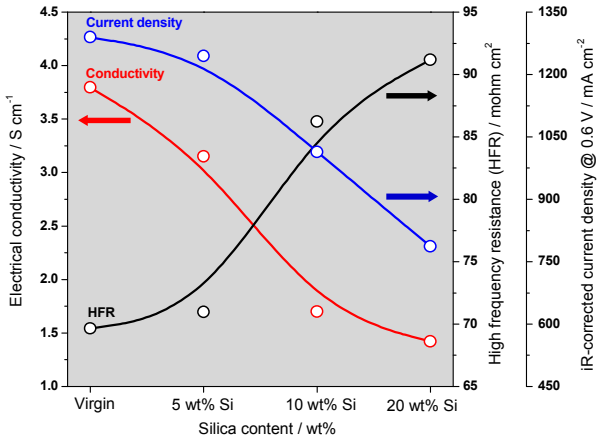

Fig. 2 Electrical conductivity of PCNF composite powder, high frequency resistance (HFR) and iR-corrected current density at 0.6 V of PCNF composite-based MEAs as a function of silica content. All of the unit cell experiments were conducted at 70 °C and 100% RH. The stoichiometric quantities of H_2 and air were 1.43 and 2.5, respectively.

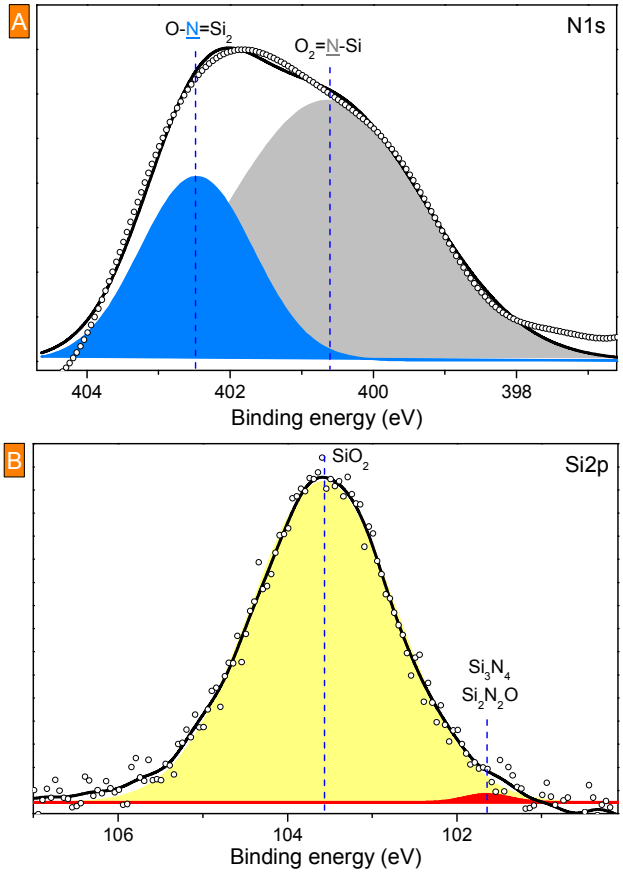

Fig. 3 XPS N 1s and Si 2p spectrums of PCNF composite powder with 5 wt% silica layer.

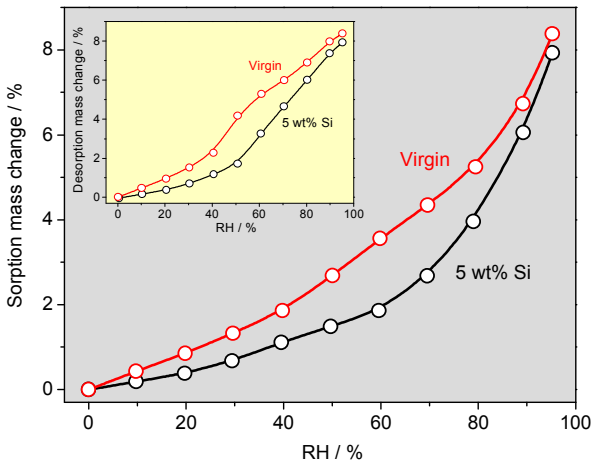

Fig. 4 Water sorption and desorption mass changes on PCNF composite with 5 wt% silica layer and virgin PCNF as a function of relative humidity (RH) condition at 25 °C.

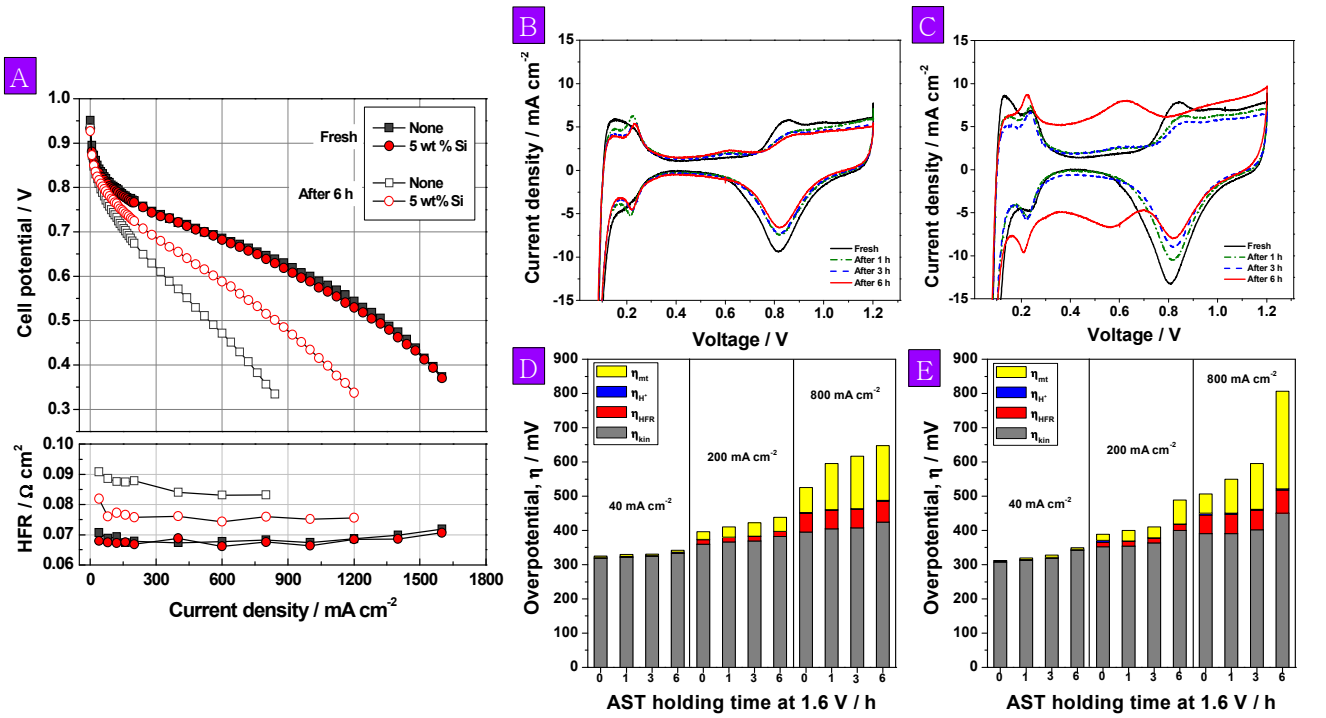

Fig. 5 Electrochemical characterization of MEAs. **A**, High frequency resistance (HFR)-uncorrected polarization curves. **B to C**, Cyclic voltammograms (CVs) of MEAs during carbon corrosion AST at 1.6 V for 6 h; B and C are the CVs of PCNF composite with 5 wt% silica layer-based and virgin PCNF without silica layer-based MEAs, respectively. **D to E**, Estimated each overpotential as a function of carbon corrosion AST time at different current densities; D and E are the estimated overpotentials of PCNF composite with 5 wt% silica layer-based and virgin PCNF without silica layer-based MEAs, respectively.